Incorporation of multiwalled carbon nanotubes into TiO$_2$ nanowires for enhancing photovoltaic performance of dye-sensitized solar cells via highly efficient electron transfer

Ji Young Ahn [a], Ji Hoon Kim [a], Kook Joo Moon [b], Jong Hyun Kim [d], Chang Sun Lee [d], Min Young Kim [d], Jae Wook Kang [c], Soo Hyung Kim [a,b,d,*]

[a] *Department of Nanofusion Technology, Pusan National University, 30 Jangjeon-dong, Geumjung-gu, Busan 609-735, Republic of Korea*
[b] *Department of Samsung Advanced Integrated Circuit, Pusan National University, 30 Jangjeon-dong, Geumjung-gu, Busan 609-735, Republic of Korea*
[c] *Department of Flexible and Printable Electronics, Chonbuk National University, 567 Baekje-daero, Deokjin-gu, Jeonju 561-756, Republic of Korea*
[d] *Department of Nanomechatronics Engineering, Pusan National University, 30 Jangjeon-dong, Geumjung-gu, Busan 609-735, Republic of Korea*

Communicated by: Associate Editor Frank Nuesch

Abstract

Multiwalled carbon nanotube (MWCNT)-embedded TiO$_2$ nanowires (NWs) were synthesized by a combination of electrospinning and calcination processes. We examined the effect of the MWCNT mass fraction in the MWCNT-TiO$_2$ composite NW-based photoelectrode on the photovoltaic properties of the resulting dye-sensitized solar cells (DSSCs). The MWCNT (5 wt%)-TiO$_2$ composite NW-based DSSC fabricated in this study showed a significantly improved short circuit current density and power conversion efficiency (PCE) compared to pure TiO$_2$ NW (i.e., MWCNT 0 wt%)-based DSSCs (the values increased from 2.91 ± 0.15 to 10.72 ± 0.21 mA/cm^2 and from $1.44 \pm 0.10\%$ to $5.03 \pm 0.35\%$, respectively). This improvement was due to an increase in rapid electron transfer and suppression in charge recombination caused by MWCNTs embedded in the TiO$_2$ matrix NWs. These specially designed MWCNT-TiO$_2$ composite NW-based photoelectrodes have great potential as an effective charge transfer medium to inherently enhance the photovoltaic performance of DSSCs.
© 2013 Elsevier Ltd. All rights reserved.

Keywords: Multiwalled carbon nanotubes; TiO$_2$ nanowires; Electrospinning; Electron transfer; Dye-sensitized solar cells

1. Introduction

Dye-sensitized solar cells (DSSCs) are very promising third-generation solar cells because of their inexpensive and relatively simple atmospheric manufacturing processes and their potentially high power conversion efficiency (PCE) (O'Regan and Grätzel, 1991). Generally, conventional DSSCs have a solid TiO$_2$ nanoparticle (NP)-accumulated photoelectrode sensitized with dye molecules, a liquid electrolyte containing an iodide/triiodide redox couple and a Pt-coated FTO glass cathode. Solid TiO$_2$ NPs with a relatively high specific surface area can absorb a large amount of dye molecules and rapidly transport photoinduced electrons (Chou et al., 2012). However, fast recombination and slow diffusion of electrons in the interfacial grain boundaries among TiO$_2$ NPs causes a decrease in the PCE of DSSCs.

Various methods have been investigated to achieve efficient electron diffusion and transport by employing TiO$_2$

---

nanotube/nanowire arrays, which enable channeled electron transfer so that the loss of photoinduced electrons among solid TiO$_2$ NPs can be significantly reduced (Law et al., 2005; Klimov, 2006; Mor et al., 2006; Zhao et al., 2010; Hwang et al., 2011; Zou et al., 2012). However, controlling the nanostructures of TiO$_2$ to enhance the electron transfer can also alter various properties of the resulting DSSCs, such as charge separation/recombination and the specific surface area of TiO$_2$ nanostructure-based photoelectrodes. As an alternative approach, nanocomposites have been suggested to enhance the electron transfer in DSSC photoelectrodes. In particular, multiwalled carbon nanotubes (MWCNTs) are regarded as promising components of nanocomposite-based DSSC photoelectrodes (Cai et al., 2012; Chang et al., 2012; Chen et al., 2012; Jang et al., 2004; Kim et al., 2006; Zhu et al., 2009). Since MWCNTs have relatively high electrical conductivity and a one-dimensional structure, they can act as an efficient charge transfer medium. However, a simple mixture of MWCNTs and TiO$_2$ NPs does not appreciably improve the photovoltaic properties of DSSCs; this is presumably because MWCNTs dispersed on the surface of TiO$_2$ NPs suppress the adsorption of dye molecules and simultaneously enhance charge recombination (Brown et al., 2008; Dang et al., 2011; Du et al., 2013; Jung et al., 2002; Peining et al., 2012). Thus, methods for effectively incorporating MWCNTs into DSSC photoelectrodes should be developed. This paper introduces the fabrication of MWCNT-TiO$_2$ composite nanowires (NWs) and discusses the effects of embedding MWCNTs in TiO$_2$ matrix NWs on the photovoltaic performance of DSSCs.

2. Experimental

2.1. Synthesis of MWCNT-TiO$_2$ composite NWs

Fig. 1a presents the schematic of the experimental setup for the fabrication of MWCNT-TiO$_2$ composite NWs. Briefly, a precursor solution composed of 2.88 g of titanium (IV) isopropoxide (TTIP, Sigma Aldrich), 16 g of N,N-dimethylformamide (DMF, Sigma Aldrich), 2.7 g of polyvinylpyrrolidone (PVP, Mw: 1,300,000, Sigma Aldrich), and various amounts of MWCNTs was sonicated for 30 min. The aforementioned precursor solution was then dispensed at a rate of 3 mL/h by using a precision syringe pump (Model No. 781100, KD Scientific). For dispensing the precursor solution, a fixed positive voltage of 25 kV was applied to the tip of the nozzle while the rotating plate was simultaneously grounded. The distance between the nozzle tip and the rotating plate was fixed at 10 cm. Subsequently, TTIP/MWCNT/PVP composite NWs were formed because of Coulombic explosion and collected on the iron mesh that covered the rotating plate. These TTIP/MWCNT/PVP composite NWs were then calcined at 450 °C for 1 h to remove the PVP templates and carry out the simultaneous thermal decomposition of the TTIP precursor into the corresponding TiO$_2$.

2.2. Fabrication of DSSCs

In order to prepare MWCNT-TiO$_2$ composite NW paste for the screen printing process, 6 g of MWCNT-TiO$_2$ composite NWs, 15 g of ethanol, 1 mL of acetic acid (CH$_3$COOH), and 20 g of terpineol were mixed in a vial and sonicated for 1 h. Three grams of ethylcellulose dissolved in 27 g of ethanol was separately prepared and subsequently added to the MWCNT-TiO$_2$ composite NW-dispersed solution, which was then sonicated for 30 min. A thin film of accumulated MWCNT-TiO$_2$ composite NWs was formed to act as a photoelectrode active layer by a screen printing process on a fluorine-doped tin oxide (FTO) glass (SnO$_2$:F, 7 Ω/sq, Philkington) with an active area of 0.6 × 0.6 cm^2, as shown in Fig. 1b and c. The resulting MWCNT-TiO$_2$ composite NW-accumulated layer formed on an FTO glass via the screen printing process was then sintered in an electric furnace at 500 °C for 30 min and subsequently immersed in anhydrous ethanol containing 0.5 mM of Ru-dye (Bu$_4$N)$_2$[Ru(Hdcbpy)$_2$-(NCS)$_2$] (N719 dye, Solaronix) for 24 h at room temperature in order to allow the dye molecules to be attached to the entire surface of the TiO$_2$ NWs. The dye-soaked MWCNT-TiO$_2$ composite NW-based photoelectrode was then rinsed with ethanol and dried in a convection oven at 80 °C for 10 min. As a counter electrode, we prepared Pt-coated FTO glass using an ion sputter (Model No. E1010, Hitachi) operated at 2.5 kV. Both the dye soaked MWCNT-TiO$_2$ composite NW-based photoelectrode and the Pt-coated counter electrode were sealed together with an inserted hot-melt polymer film (60-μm thick, Surlyn, DuPont), and an iodide-based liquid electrolyte (AN-50, Solaronix) was then injected into the interspace between the electrodes.

2.3. Characterization of materials and photovoltaic devices

The physical properties of the resulting MWCNT-TiO$_2$ composite NWs fabricated in this study were characterized using various techniques, including scanning electron microscopy (SEM, S-4200, Hitachi) operated at ~15 kV, transmission electron microscopy (TEM, JEM 2100F, JEOL) operated at ~100 kV, and X-ray diffraction (XRD, Empyrean series2, PANalytical). The current–voltage (J–V) characteristics of the DSSCs fabricated in this study were measured under AM 1.5 simulated illumination with an intensity of 100 mW/cm^2 (PEC-L11, Pecell Technologies Inc.). The intensity of sunlight illumination was calibrated using a standard Si photodiode detector with a KG-5 filter. The J–V curves were automatically recorded using a Keithley SMU 2400 source meter by illuminating the DSSCs.

3. Results and discussion

MWCNT-TiO$_2$ composite NWs were formed using electrospinning and subsequent calcination processes. The PVP
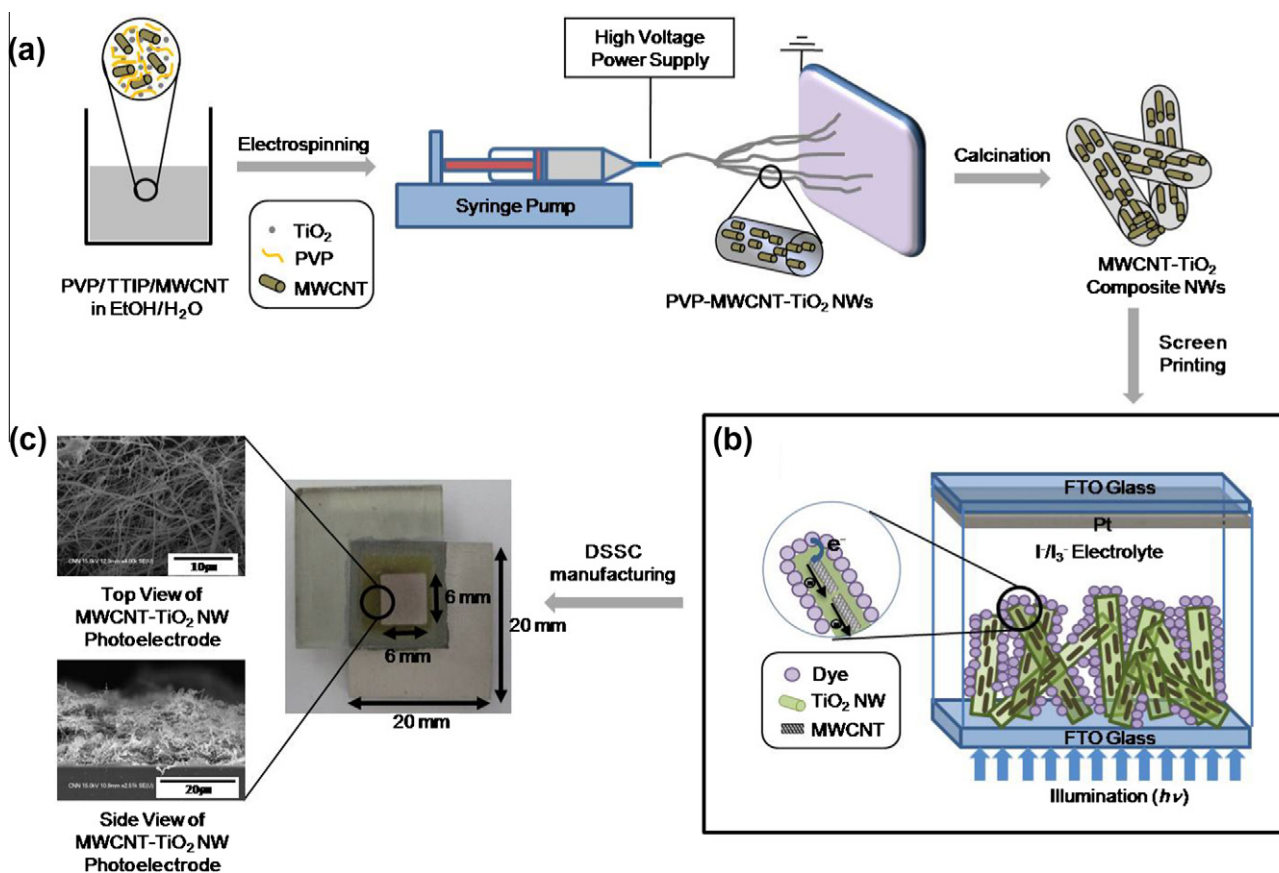
Fig. 1. (a) Schematic of the experimental setup for the fabrication of MWCNT-TiO$_2$ composite NWs, (b) schematic of electron transport in the MWCNT-TiO$_2$ composite NW-based DSSC, and (c) picture of DSSC manufactured in this study and SEM images of MWCNT-TiO$_2$ composite NW-based photoelectrode.

templates in the MWCNT-TiO$_2$ composite NWs were confirmed via SEM analysis to play a key role in securing NW structures for the as-prepared PVP–MWCNT-TiO$_2$ composite NWs (see Fig. 2a and b). The average diameter of the as-prepared PVP–MWCNT-TiO$_2$ composite NWs was approximately ~243 ± 20 nm, as shown in Fig. 2a. However, after removal of the PVP templates by calcination, the diameter of the MWCNT-TiO$_2$ composite NWs was observed to be ~87 ± 2 nm, as shown in Fig. 2b. A closer look at a single MWCNT-TiO$_2$ composite NW, as shown in Fig. 2c and d, found that the MWCNTs were axially aligned along the TiO$_2$ matrix NW. The presence of MWCNTs in the TiO$_2$ NWs was not clearly observed in TEM images because of the relatively high transmittance of electrons in the MWCNTs, as shown in Fig. 2e. However, the high-resolution TEM (HRTEM) image for the thin film of an MWCNT-embedded TiO$_2$ NW sample prepared using a focused ion beam (FIB), as shown in Fig. 2f, confirmed that the MWCNTs clearly resided inside the TiO$_2$ matrix NW.

Fig. 3 shows the XRD patterns of MWCNT-TiO$_2$ composite NWs calcined at 450 °C. The resulting phase composition of MWCNT-TiO$_2$ NWs fabricated by this approach was calculated to be anatase:rutile = 63:37. The phase composition was calculated from the integrated intensities of the anatase and rutile peaks.

In order to examine the effect of MWCNTs embedded inside the TiO$_2$ NWs on the photovoltaic performance of DSSCs, we fabricated various DSSCs composed of TiO$_2$ NWs embedded with various amounts of MWCNTs. Table 1 lists the photovoltaic characteristics of the MWCNT-TiO$_2$ composite NW-accumulated photoelectrodes, and Fig. 4 shows the J–V curves of the fabricated DSSCs measured under AM 1.5 illumination (100 mW/cm^2) as a function of the MWCNT mass fraction in the TiO$_2$ NWs. The J_{sc} values of the DSSCs increased from 2.91 ± 0.15 mA/cm^2 for pure TiO$_2$ NWs (0 wt% MWCNTs) to 10.72 ± 0.21 mA/cm^2 for TiO$_2$ NWs embedded with 5 wt% MWCNTs; this considerably improved the PCE from 1.44 ± 0.10% to 5.03 ± 0.35%. The improvement in the J_{sc} of DSSCs by increasing the mass fraction of MWCNTs embedded in the TiO$_2$ NWs resulted from the acceleration of electron transfer and the minimization of the loss of photoinduced electrons that recombined with holes on the TiO$_2$ NWs. However, the open circuit voltage (V_{oc}) and fill factor (FF) of DSSCs constructed from MWCNT-embedded TiO$_2$ NWs did not show any appreciable changes, as compared to those of DSSCs constructed from pure TiO$_2$ NWs without
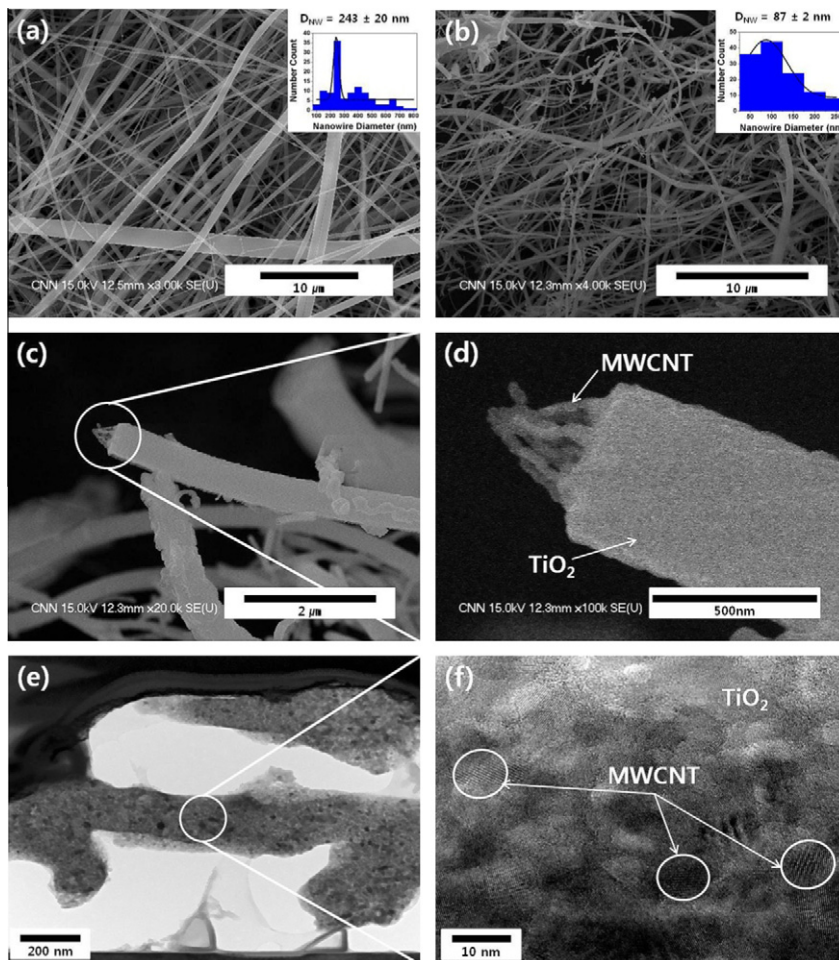
Fig. 2. SEM images of (a) as-prepared electrospun PVP–MWCNT-TiO$_2$ NWs, (b) MWCNT-TiO$_2$ composite NWs after calcination, (c) LRSEM image of MWCNTs exposed on the surface of a TiO$_2$ NW, and (d) HRSEM image of MWCNTs and a TiO$_2$ NW. TEM images of (e) thin layer of MWCNT-TiO$_2$ NW prepared by using a focused ion beam (FIB) and (f) MWCNTs embedded in a TiO$_2$ matrix NW.
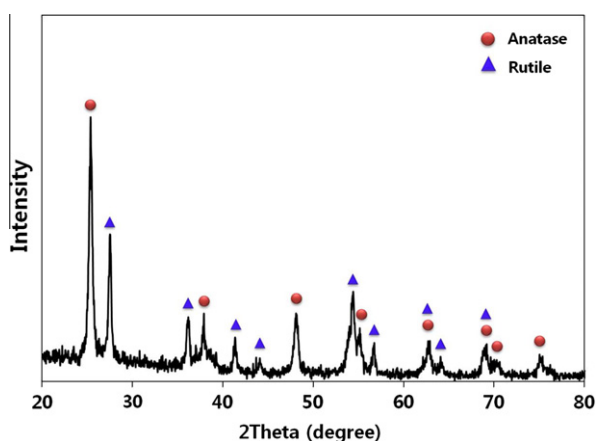

Fig. 3. XRD patterns of the resulting TiO$_2$ NWs calcined at 450 °C for 1 h.

MWCNTs. This suggests that the photovoltaic conversion properties and interfacial structure of the MWCNT-TiO$_2$ composite NW-based layer and liquid electrolyte are very similar for all DSSCs fabricated by this approach.

The charge transfer-related internal resistance in the MWCNT-TiO$_2$ composite NW-based photoelectrode was measured by electrochemical impedance spectroscopy (EIS). Fig. 5a shows the Nyquist plots for MWCNT (0–10 wt%)-TiO$_2$ composite NW-based photoanodes. Generally, the Nyquist plots exhibited three semicircles in the DSSCs: (i) redox reaction at the Pt counter electrode in the high-frequency region, (ii) electron transfer at the TiO$_2$/dye/electrolyte interface in the middle-frequency region, and (iii) carrier transport by ions within the electrolytes in the low-frequency region. However, with the proposed approach, we were able to observe very small semicircles at the low-frequency region and large semicircles at the middle-frequency region for all the DSSCs. This suggests that the resistance to ion transport in the electrolyte is very weak and that the charge transfer resistance in the MWCNT-TiO$_2$ composite NW photoelectrode is very strong. Fig. 5a clearly shows that the diameter of the semicircles decreases with an increase in the amount of MWCNTs (0–5 wt%) embedded in the TiO$_2$ matrix NWs; this suggests that the presence of MWCNTs in the TiO$_2$ NWs reduces the charge transfer resistance at the TiO$_2$/dye/electrolyte interface. Since MWCNTs have relatively

Table 1
Summary of photovoltaic characteristics of MWCNT-TiO$_2$ composite NW-accumulated photoelectrodes in DSSCs.

wt% MWCNTs in TiO$_2$ NW	t_e (ms)	J_{sc} (mA/cm^2)	V_{oc} (V)	FF	PCE (%)
0.0	1	2.91 ± 0.15	0.70 ± 0.01	0.71 ± 0.01	1.44 ± 0.10
0.1	2	3.94 ± 0.08	0.67 ± 0.01	0.69 ± 0.02	1.81 ± 0.24
0.2	4	5.38 ± 0.33	0.69 ± 0.01	0.69 ± 0.01	2.56 ± 0.11
0.5	5	6.38 ± 0.05	0.71 ± 0.01	0.71 ± 0.01	3.20 ± 0.08
1.0	10	7.88 ± 0.25	0.67 ± 0.03	0.70 ± 0.02	3.67 ± 0.24
2.0	13	8.96 ± 0.18	0.69 ± 0.01	0.70 ± 0.01	4.48 ± 0.27
5.0	25	10.72 ± 0.21	0.67 ± 0.01	0.70 ± 0.02	5.03 ± 0.35
10.0	12	8.00 ± 0.43	0.71 ± 0.02	0.73 ± 0.05	4.13 ± 0.21
20.0	8	7.23 ± 0.11	0.71 ± 0.03	0.71 ± 0.01	3.62 ± 0.16

Note: electron lifetime (t_e), short circuit current (J_{sc}), open circuit voltage (V_{oc}), fill factor (FF), power conversion efficiency (PCE).
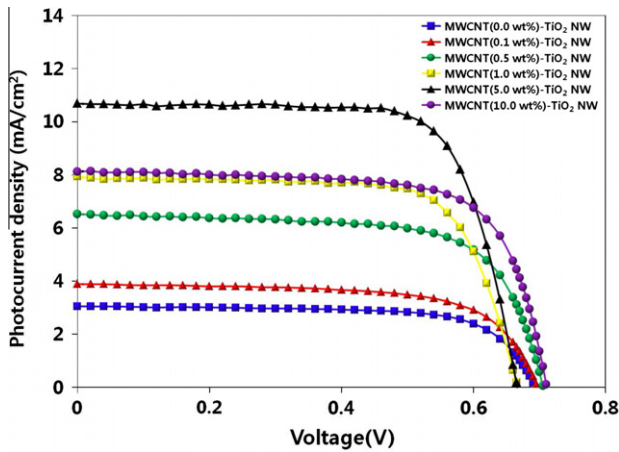

Fig. 4. *J–V* characteristics of MWCNT-TiO$_2$ composite NW-based photoelectrodes of DSSCs.

high electrical conductivity, the photogenerated electrons can rapidly diffuse and transport through the MWCNTs embedded in the TiO$_2$ NWs, which leads to a lower resistance and a higher PCE (see Table 1 and Fig. 4).

The electron lifetime can be calculated by the following equation:

$$\tau = (2\pi f_{max})^{-1} \qquad (1)$$

where f_{max} is the maximum frequency of the middle-frequency peak in the Bode phase plot, as shown in Fig. 5b. The Bode phase plots show the various frequency peaks of the charge transfer process for various MWCNT-TiO$_2$ composite NW-based DSSC photoelectrodes. The maximum frequency shifted to a lower frequency with an increase MWCNT content in the MWCNT-TiO$_2$ composite NWs, and the electron lifetime was calculated to be 1, 5, 10, and 25 ms for 0, 0.5, 1, and 5 wt% MWCNTs, respectively, in the MWCNT-TiO$_2$ composite NWs. It should be noted that the increase in charge resistance and the decrease in electron lifetime at considerably high MWCNT content (>10 wt%) in MWCNT-TiO$_2$ composite NWs is presumably attributed to charge recombination, which can occur in highly aggregated MWCNTs exposed to the TiO$_2$ NW surface such that photogenerated electrons are easily lost by contact with the electrolyte, dye, and TiO$_2$. EIS analysis confirmed that the presence of an optimum
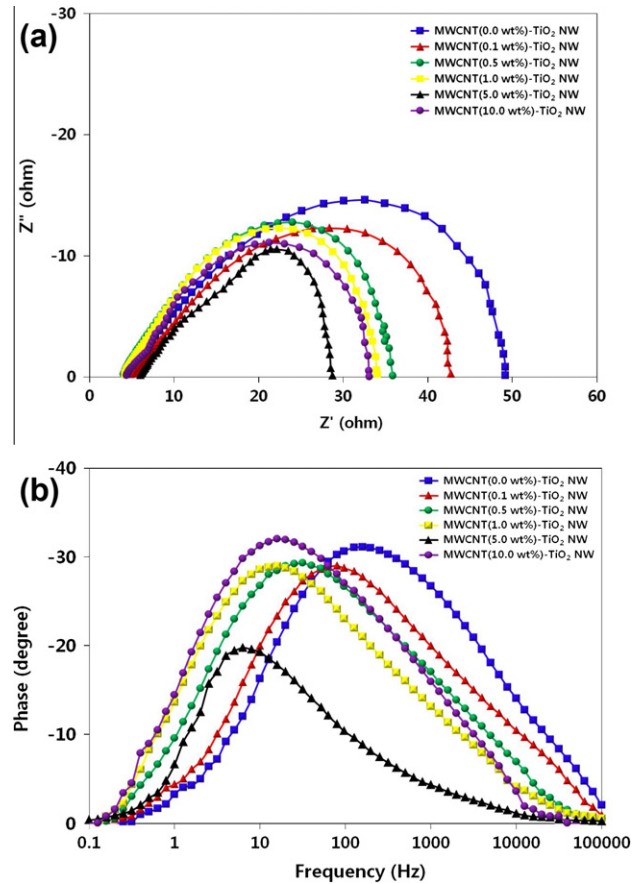

Fig. 5. (a) Nyquist plots and (b) Bode plots of DSSCs composed of various MWCNT content in the MWCNT-TiO$_2$ composite NW-based photoelectrodes of DSSCs.

amount of MWCNTs in the MWCNT-TiO$_2$ composite NWs in the photoelectrodes can reduce electron recombination and simultaneously accelerate electron transfer; thus, these MWCNT-TiO2 composite NW-accumulated photoelectrodes exhibit an effective light harvesting performance in DSSCs.

4. Conclusions

We described a simple and viable electrospinning method for the synthesis of MWCNT-TiO$_2$ composite NWs. The method facilitates the formation of TiO$_2$ NWs

embedded with MWCNTs that can rapidly transport photogenerated electrons through TiO_2 matrix NWs and simultaneously suppress charge recombination between the electron and the dye or the redox couple when used in DSSC photoelectrodes. The photovoltaic performance of DSSCs improved significantly when the amount of MWCNTs in the MWCNT-TiO_2 composite NW-accumulated photoelectrode was increased to up to ~5 wt%. This suggests that the proposed MWCNT-TiO_2 composite NW-based photoelectrode might help to improve the inherent photovoltaic performance of DSSCs by efficient light harvesting and promotion of electron transfer.

Acknowledgement

References

Brown, P., Takechi, K., Kamat, P.V., 2008. J. Phys. Chem. C 112, 4776–4782.

Cai, F., Chen, T., Peng, H., 2012. J. Mater. Chem. 22, 14856–14860.

Chang, M., Wu, L., Li, X., Xu, W., 2012. J. Mater. Sci. Technol. 28 (7), 594–598.

Chen, T., Qui, L., Cai, Z., Gong, F., Yang, Z., Wang, Z., Peng, H., 2012. Nano Lett. 12, 2568–2572.

Chou, C.S., Guo, M.G., Liu, K.H., Chen, Y.S., 2012. Appl. Energy 92, 224–233.

Dang, X., Yi, H., Ham, M.H., Qi, J., Yun, D.S., Ladewski, R., Strano, M.S., Hammond, P.T., Belchel, A.M., 2011. Nature Nanotech. 6, 377–384.

Du, P., Song, L., Xiong, J., Li, N., Wang, L., Xi, Z., Wang, N., 2013. Electrochim. Acta 87, 651–656.

Hwang, H.Y., Prabu, A.A., Kim, D.Y., Kim, K.J., 2011. Solar Energy 85, 1551–1559.

Jang, S.R., Vittal, R., Kim, K.J., 2004. Langmuir 20, 9807–9810.

Jung, K.H., Hong, J.S., Vittal, R., Kim, K.J., 2002. Chem. Lett. 31, 864–865.

Kim, S.L., Jang, S.R., Vittal, R., Lee, J., Kim, J.K., 2006. J. Appl. Electrochem. 36, 1415–1426.

Klimov, V.I., 2006. J. Phys. Chem. B 110, 16827–16845.

Law, M., Greene, L.E., Johnwon, J.C., Saykally, R., Yang, P., 2005. Nature Mater. 4, 455–459.

Mor, G.K., Shankar, K., Paulose, M., Varghese, O.K., Grimes, C.A., 2006. Nano Lett. 6, 215–218.

O'Regan, B., Grätzel, M., 1991. Nature 353, 737–740.

Peining, Z., Nair, A.S., Shengyuan, Y., Shengjie, P., Elumalai, N.K., Ramakrishna, S., 2012. J. Photochem. Photobiol. A: Chem. 231, 9–18.

Zhao, T.Y., Liu, Z.Y., Nakata, K., Nishimoto, S., Murakami, T., Zhao, Y., Jiang, L., Fujishima, A., 2010. J. Mater. Chem. 20, 5095–5099.

Zhu, H., Wei, J., Wang, K., Wu, D., 2009. Sol. Energy Mater. Sol. Cells 93, 1461–1470.

Zou, Y., Li, D., Sheng, X., Wang, L., Yang, D., 2012. Solar Energy 86, 1359–1365.